Stratospheric and Mesospheric Kelvin Waves Simulated by the GFDL "SKYHI" General Circulation Model

Y. HAYASHI, D. G. GOLDER AND J. D. MAHLMAN

Geophysical Fluid Dynamics Laboratory/NOAA, Princeton University, Princeton, NJ 08542

(Manuscript received 4 November 1983, in final form 29 March 1984)

ABSTRACT

A space–time spectral analysis is made of large-scale equatorial disturbances simulated by the 40-level, 5° latitude GFDL "SKYHI" general circulation model with annual mean conditions. Three kinds of eastward moving waves with wavenumbers 1–2 are found in the lower and upper stratosphere and mesosphere. These waves are characterized by small meridional winds and an eastward tilt with height and are identifiable with observed Kelvin waves. A time–height section reveals their vertical group propagation.

The lower stratospheric Kelvin wave is associated with periods of 10–30 days (eastward phase speed 15–46 m s^{-1}) for wavenumber 1 and a vertical wavelength of ~10 km, corresponding to that observed in 1968 by Wallace and Kousky. The upper stratospheric Kelvin wave is associated with periods of 5–7 days (66–92 m s^{-1}) for wavenumber 1 and a vertical wavelength of ~20 km, corresponding to that observed by Hirota. The mesospheric Kelvin wave is associated with periods of 3–4 days (115–154 m s^{-1}) for wavenumber 1 and a vertical wavelength of ~40 km, corresponding to that recently discovered by Salby and others. All these Kelvin waves transport energy and eastward momentum upward and contribute to the maintenance of the eastward flow.

In addition, gravity waves of zonal wavenumbers 1–30 and periods of 0.7–2 days have been found, particularly in the model's equatorial stratosphere and mesosphere. Their eastward and westward moving components transport eastward and westward momentum upward and contribute to the momentum balance as much as, or even more than, Kelvin waves with periods longer than two days.

1. Introduction

As reviewed by Wallace (1973), Yanai (1975) and Hirota (1980), there is considerable observational evidence of eastward moving equatorial waves associated with wavenumber 1 with periods near 15 days in the lower stratosphere and periods of ~5–10 days in the upper stratosphere.

The lower stratospheric wave with periods near 15 days found by Wallace and Kousky (1968) is characterized by the absence of a meridional component and tilts eastward with height with vertical wavelength of ~5–10 km. This wave is interpreted as an equatorial Kelvin wave discussed theoretically by Matsuno (1966) and Holton and Lindzen (1968). It transports eastward (westerly) momentum upward as observed by Kousky and Wallace (1971) and is likely to play an important role in the quasi-biennial oscillation of the zonal mean wind, as suggested theoretically by Lindzen and Holton (1968) and Holton and Lindzen (1972).

The upper stratospheric wave with periods of ~5–10 days found by Hirota (1978, 1979) is also likely to be a Kelvin wave and is associated with a larger vertical wavelength (~20–25 km) than the lower stratospheric Kelvin wave. This upper stratospheric Kelvin wave may play an important role in the semiannual oscillation in the tropical middle atmosphere through a possible upward transport of eastward momentum as suggested theoretically by Dunkerton (1979, 1982).

Salby *et al.* (1984) have recently found, in addition to the upper stratospheric Kelvin wave, mesospheric Kelvin waves that are associated with wavenumber 1 and 2. The wavenumber 1 component had an eastward moving period of 3.5–4.0 days, and an eastward tilt of ~40 km vertical wavelength, while the wavenumber 2 component had an eastward moving period of 3.8–4.3 days, and an eastward tilt of ~20 km vertical wavelength.

Hayashi (1974) and Hayashi and Golder (1980) found, among other equatorial planetary waves, Kelvin waves associated with wavenumber 1 and a period of 15 days in an 11-level GFDL general circulation model with seasonal variation, developed by Manabe *et al.* (1974). However, this model does not have upper stratospheric levels.

Mahlman and Sinclair (1980) have developed a 40-level 9° latitude mesh "SKYHI" model and found that the semiannual oscillation is reasonably well simulated in the presence of a seasonal variation [for model details see Fels *et al.* (1980) and Andrews *et al.* (1983).] They have also developed a 40-level 5° latitude mesh model without seasonal variations (Andrews *et al.*, 1983) and with seasonal variations (Mahlman and Umscheid, 1983). Although the semiannual oscillation

does not occur without seasonal variations, westerlies do prevail over the equatorial stratosphere and mesosphere. Andrews *et al.* (1983) have made Eliassen–Palm diagnostics of this model and found, in particular, that the Eliassen–Palm flux divergence in the equatorial stratosphere and mesosphere is primarily due to the convergence of vertical eddy momentum flux. It is of importance to examine what kind of disturbances contributed to this eddy momentum flux convergence.

This paper presents a space–time spectral analysis of the same 5° latitude mesh model experiment investigated by Andrews *et al.* (1983) and compares the results with an observational analysis of Kelvin waves by Salby *et al.* (1984). Since this model has annual mean conditions and fails to simulate semiannual and quasi-biennial oscillations, it may not be suitable for a direct comparison with observations. Nevertheless, this study is the first to detect three types of Kelvin waves in a general circulation model. The advantage of a model is that the vertical flux of momentum and energy can be directly calculated from the model data. It is also possible to resolve waves with periods shorter than two days by the use of six-times-daily data which have been stored for a one-month model sampling period, whereas only twice-daily data are available from polar-orbiting satellite data and are subject to space–time aliasing errors as discussed by Salby (1982). In Sections 2 and 3, a space–time spectral analysis has been made by the use of the once-daily data and the six-times-daily data. Conclusions and remarks are given in Section 4. The Appendix summarizes a method (Hayashi, 1977b) of partitioning space–time power spectra into standing and traveling parts.

2. Analysis of daily data

a. Method

The wavenumber-frequency characteristics and structure of disturbances are examined by a space–time spectral analysis (see Hayashi, 1982 for a review of the method and its applications). Space–time power spectra are estimated by the use of the univariate maximum entropy (autoregressive) method (see Hayashi, 1977a) which results in fine frequency resolutions even for a short time record. Space–time cospectra, phase difference and coherence are estimated by the bivariate maximum entropy method (see Hayashi, 1981). The bandwidth of frequency averaging is 1/30 day^{-1}. The data set used here is the once-daily data for 30 days which was obtained by averaging over six samples a day. This averaging filters aliasing errors from 0.33–1-day periods almost completely and reduces those from 1–2 day periods.

b. Mean zonal wind

Figure 1 shows the latitude–height distribution of the mean zonal wind (30-day average) of the model

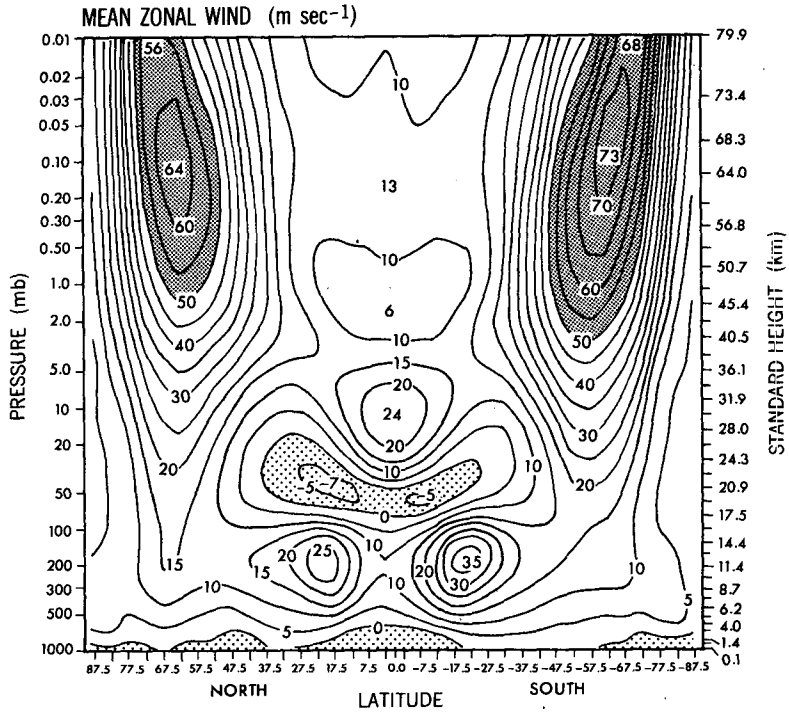

FIG. 1. Latitude-height distribution of mean zonal wind (m s^{-1}) of the 40-level, 5° mesh GFDL SKYHI general circulation model with annual mean condition. The period of averaging is 30 days with sampling taken six times per day (after Andrews *et al.*, 1983). The standard height indicates the level of the finite-difference model.

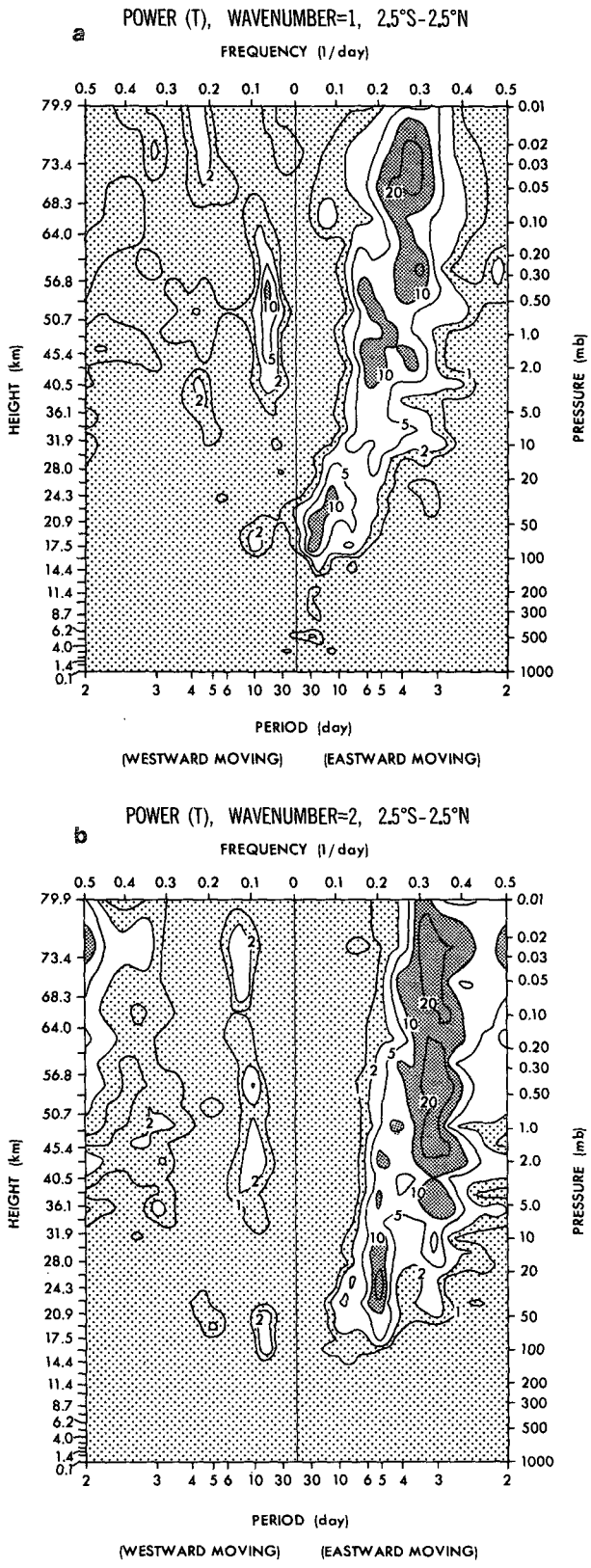

FIG. 2. Frequency–height distribution (2.5°S–2.5°N) of space–time power spectral density (K^2 day) of temperature for wavenumber 1(a) and 2(b). In this and all other figures, heights given are standard atmosphere values for the model pressure levels.

with annual mean conditions. The levels of model are indicated by the standard height corresponding to the model pressure levels. In the tropics, westerlies prevail except near 50 mb and the lower troposphere. These westerlies attain local maxima around the 30 and 60 km levels. This wind distribution more or less resembles the westerly phase of the observed semiannual oscillations (see Hamilton, 1982, Fig. 1), while the Salby *et al.* (1984) analysis shows easterlies over the equator below 50 km during the period 31 January–6 February 1979.

It should be mentioned that the subtropical jet in the troposphere occurs about 10° too close to the equator and that easterlies appear at the surface in the Northern Hemisphere middle latitudes. These defects are due to the coarse horizontal resolution and are largely alleviated in the current SKYHI model with higher horizontal resolutions. These defects will not, however, affect equatorial Kelvin waves which are probably generated within the tropics. Hayashi and Golder (1978) demonstrated by a 13-level general circulation model that the stratospheric Kelvin wave is hardly affected when midlatitude disturbances are eliminated, though it diminishes when condensational heating is eliminated.

c. *Vertical structure*

Figure 2a shows the frequency–height distribution averaged over two latitudes (2.5°S and 2.5°N) of the

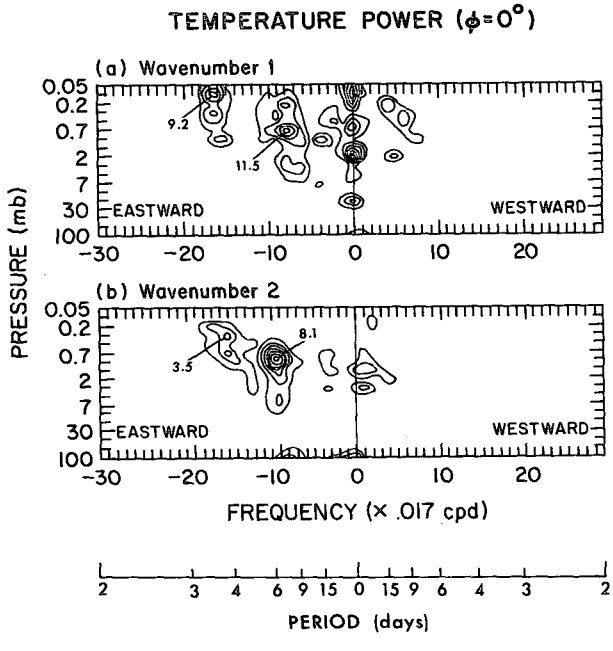

FIG. 3. Frequency–height distribution (equator) of space–time power spectral density of observed temperature (January–February 1979) for wavenumber 1(a) and 2(b). Contour increment is 0.04 × 58 K^2 day for wavenumber 1 and 0.02 × 58 K^2 day for wavenumber 2 (after Salby *et al.*, 1984).

space–time power spectral density of temperature for wavenumber 1. Three major spectral peaks can be found at eastward moving periods of 10–30, 5–7 and 3–4 days, at levels of 15–25, 40–55 and 50–80 km respectively. These three periods agree with those of Kelvin waves observed by Wallace and Kousky (1968), Hirota (1979) and Salby *et al.* (1984) respectively. Fig. 2b shows that these dominant periods are almost halved for wavenumber 2, being consistent with Kelvin waves whose frequency is proportional to their wavenumber (i.e., nondispersive).

In order to compare the present results with observations, Fig. 3 reproduces the observed spectra (January–February) of Salby *et al.* (1984) corresponding to Fig. 2. Although the present model has annual mean conditions, the power spectral densities at the eastward moving periods 5–7 and 3–4 days are in close agreement with those observed except for wavenumber 2 and period 3–4 days.

Figure 4 shows the frequency–height distribution of the geopotential for wavenumber 1. In contrast to temperature (Fig. 2a), the power spectra of the geopotential at the eastward moving periods of 20–30 days in the lower stratosphere is extremely small compared to those at the eastward moving periods of 3–4 days in the mesosphere. The difference between the temperature and geopotential spectra is hydrostatically consistent

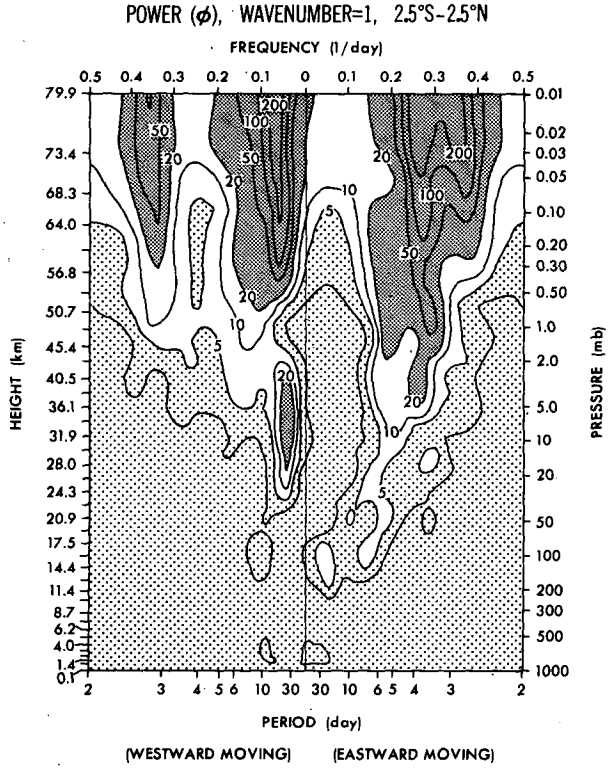

FIG. 4. Frequency–height distribution (2.5°S–2.5°N) of space–time power spectral density (10^4 m^4 s^{-4} day) of geopotential for wavenumber 1.

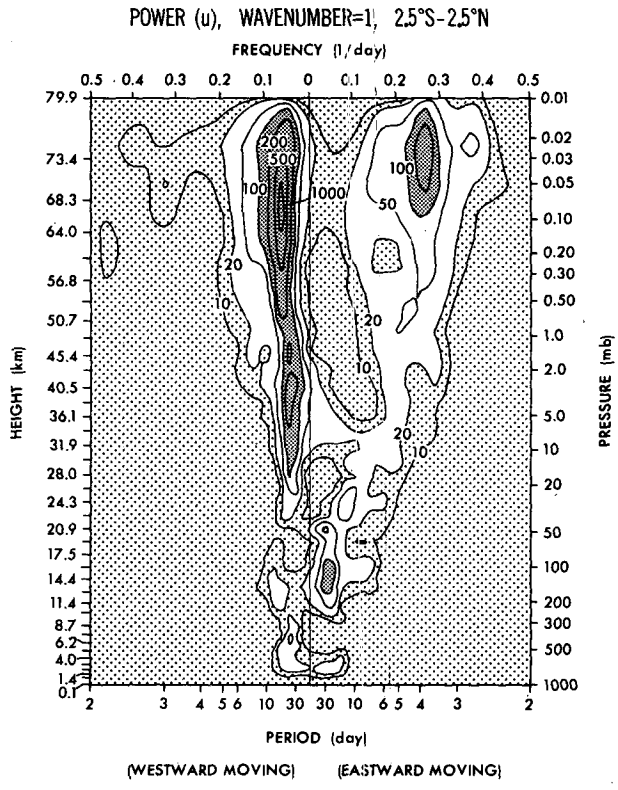

FIG. 5. Frequency–height distribution (2.5°S–2.5°N) of space–time power spectral density (m^2 s^{-2} day) of zonal velocity component for wavenumber 1.

with the fact that the lower stratospheric wave has a steeper vertical tilt than the mesospheric wave as will be illustrated later. In contrast to temperature, pronounced spectral peaks of geopotential appear not only for the eastward moving component but also for the westward moving one. This difference is also hydrostatically consistent with the fact (not illustrated) that the eastward moving component has a steeper vertical tilt than the westward moving one. The latter component corresponds to the observed (Madden, 1978, 1979; Madden and Labitzke, 1981) and simulated (Hayashi and Golder, 1983) 16-day Rossby waves which are theoretically interpreted as external Rossby waves (e.g., Salby, 1981).

Figure 5 shows the frequency–height distribution of the zonal velocity for wavenumber 1. The large amplitude of the zonal velocity of low frequency oscillations is consistent with the fact that the approximate balance $\partial u/\partial t \approx -\partial\phi/\partial x$ holds near the equator where the Coriolis force fv is negligible.

Figure 6 shows the frequency–height distribution (wavenumbers 1–2) of the vertical flux of energy $(-\overline{\phi'\omega'})$ divided by $p^{1/2}$ for convenience in contouring, where ϕ, ω and p are the geopotential, vertical pressure velocity and pressure respectively. It should be noted that the eastward moving component is associated with a predominantly positive (upward) flux of energy above

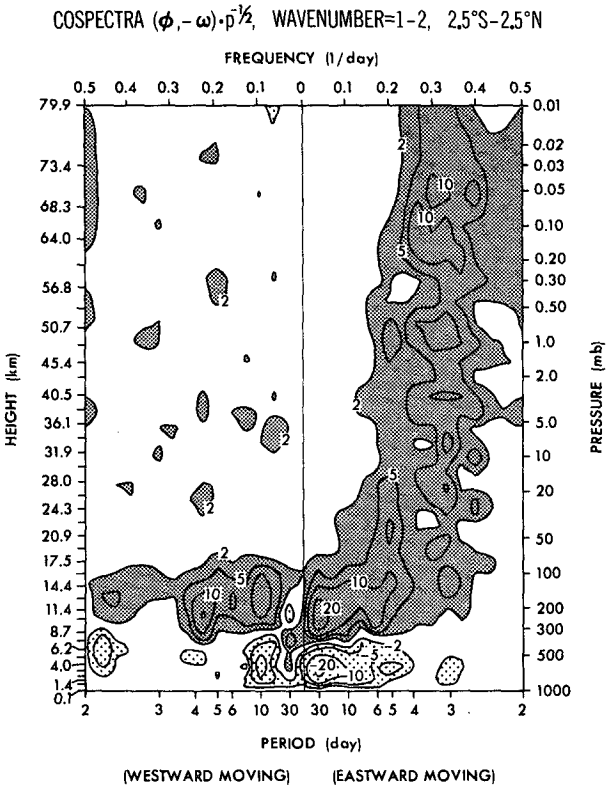

FIG. 6. Frequency–height distribution (2.5°S–2.5°N) of space–time cospectral density (10^{-4} W kg^{-1} mb$^{1/2}$ day) of vertical flux of energy ($-\overline{\phi'\omega'}p^{-1/2}$) for wavenumbers 1–2.

7 km, while the westward moving component is associated with a smaller flux above 7 km. The reversal of the direction of the energy flux at 7 km suggests that the wave energy source exists near this level.

Figure 7 shows the frequency–height distribution (wavenumbers 1–2) of the vertical flux of zonal momentum ($-\overline{u'\omega'}$) divided by p for convenience in contouring. It is seen that the eastward moving component is associated with a positive flux above 10 km, while the westward moving component is associated with a smaller flux. It is also of interest to note in Fig. 7 that $-\overline{u'\omega'}$ decays with height in such a way that $-\overline{u'\omega'}p^{-1}$ ($\approx\overline{u'w'}$) is more or less constant in the mesosphere. This result may be related to the nonlinear breaking (saturation) of planetary waves as discussed theoretically by McIntyre and Palmer (1983).

The above spectral analysis suggests that the three major spectral peaks found in the space–time power spectral density of temperature (Fig. 2a) are due to Kelvin waves which transport both energy and westerly momentum upward in the stratosphere and mesosphere. Fig. 8a shows vertical distributions (2.5°N) of the space–time amplitude, phase difference and coherence (frequency band width = 1/30 day^{-1}) of temperature for wavenumber 1 and an eastward moving period of 15 days. The amplitude is largest at the 21 km level and decays rapidly with height. Around this level (15–30 km), the phase line tilts eastward with height and is associated with a vertical wavelength of ~10 km. This feature and the order of magnitude of the amplitude are in agreement with those of the lower stratospheric Kelvin wave observed by Wallace and Kousky (1968) and others. The coherence with respect to the 21 km level is close to 1.0 between the 15 and 30 km levels.

Figure 8b is the same as Fig. 8a except for an eastward moving period of 5 days. The amplitude is largest at the 43 km level. Around this level (30–60 km), the phase line tilts eastward with height and is associated with a vertical wavelength of about 20 km. This feature and the magnitude of the amplitude are in close agreement with those of the upper stratospheric Kelvin wave observed by Hirota (1979) and Salby *et al.* (1984). The vertical coherence with respect to 43 km is close to 1.0 between the 30 and 60 km levels.

Figure 8c is the same as Fig. 8a except for an eastward moving period of 3.8 days. It should be noted that the amplitude for 3.8 and 5.0 day periods estimated from once-daily data averaged over six samples per day oscillates greatly with height. It turns out that this amplitude oscillation is due to aliasing errors from oscillations with periods ~ 1–2 days that are not com-

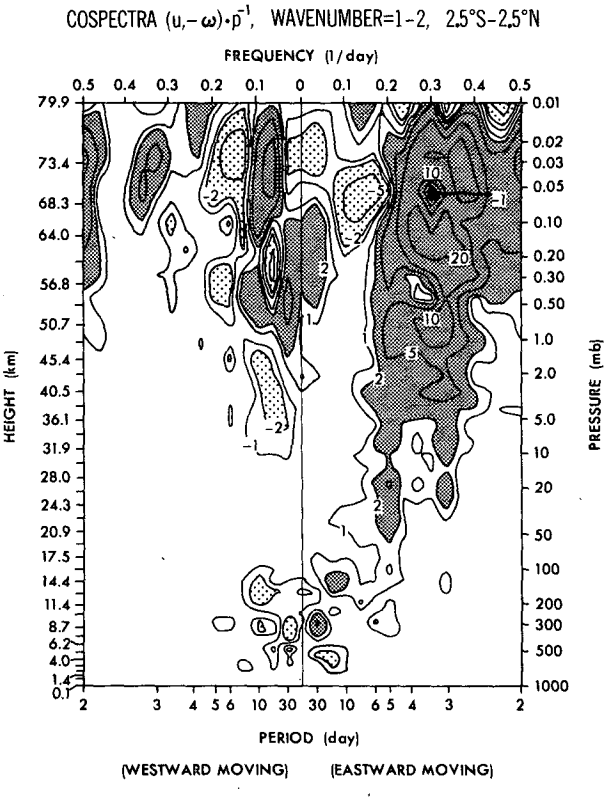

FIG. 7. Frequency–height distribution (2.5°S–2.5°N) of space–time cospectral density (10^{-6} m s^{-2} day) of the vertical flux of zonal momentum ($-\overline{u'\omega'}p^{-1}$) for wavenumber 1–2.

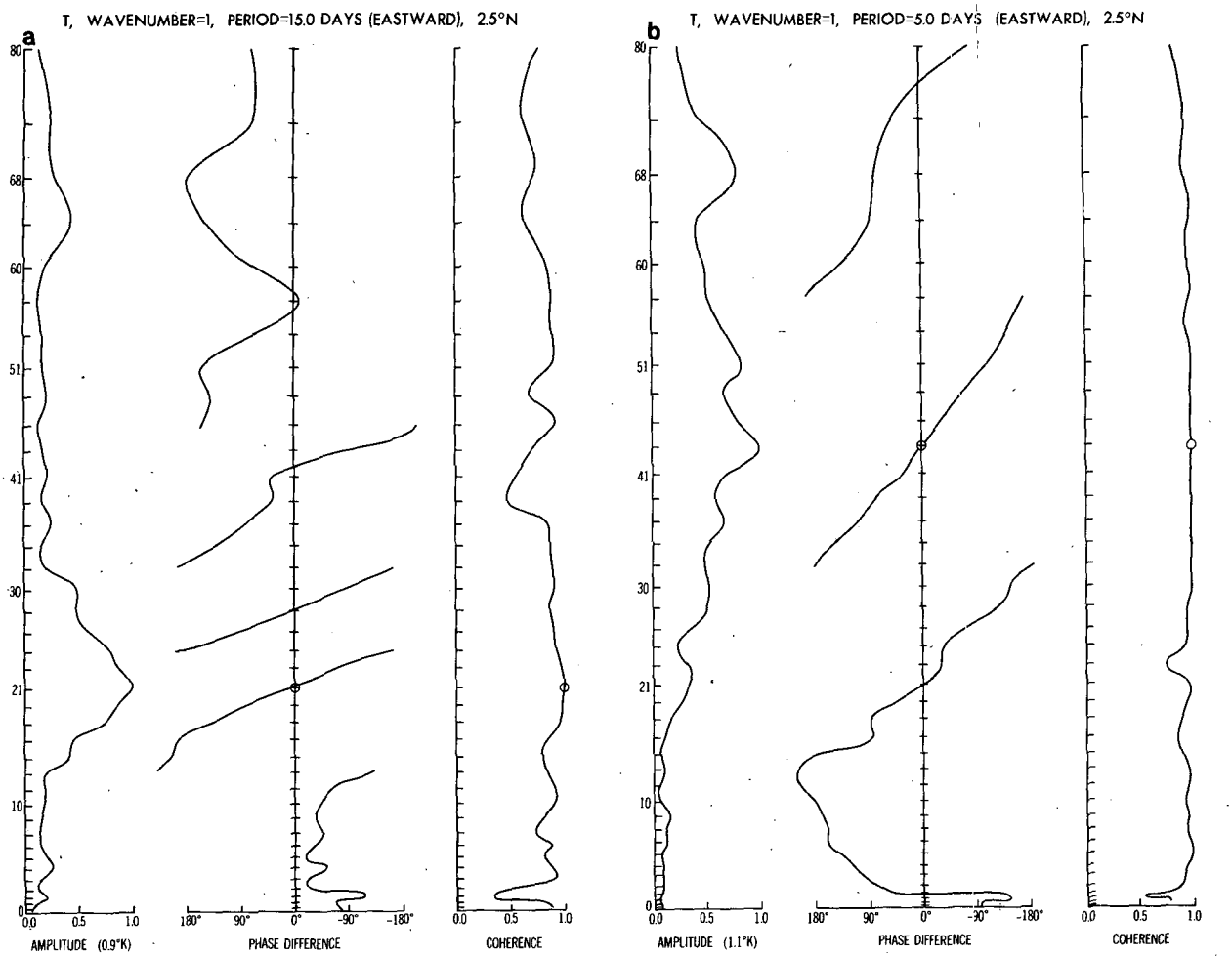

FIG. 8. Vertical profile (2.5°N) of space-time amplitude, phase difference and coherence of the temperature (wavenumber 1). The units of amplitude over frequency width 30^{-1} day^{-1} are parenthesized. The reference levels are indicated by circles. Eastward moving periods of (a) 15 days, (b) 5 days and (c) 3.8 days.

pletely eliminated by the averaging. This oscillation is reduced in the amplitude estimated from six-times-daily data without averaging as indicated in Fig. 8c. This oscillation can also be smoothed by the use of a longer time record. The amplitude is largest at the 73 km level. Below this level (45–68 km), the phase line tilts eastward with height and is associated with a vertical wavelength of about 40 km. This feature and the magnitude of the amplitude are in close agreement with those of the upper stratospheric Kelvin wave recently discovered by Salby *et al.* (1984). The vertical coherence with respect to the 57 km level is close to 1.0 between the 45 and 68 km levels.

It is of interest to visualize how these waves oscillate and propagate vertically. Figs. 9a and 9b show the time–height distribution of the wavenumber 1 and 2 components of temperature at 0° longitude (i.e., zonal cosine coefficient) averaged over two latitudes (2.5°S and 2.5°N). The oscillations with periods corresponding to the spectral peaks in Fig. 2 are clearly detectable. In addition to downward phase propagations above 15 km, upward group propagation is detectable when large positive and large negative values are traced. This group propagation suggests that these waves are excited in the troposphere by forcing associated with a broad frequency range.

d. Latitudinal structure

The frequency–latitude distribution of the space–time power spectral density of temperature for wavenumber 1 is shown by Fig. 10. According to Fig. 10a (47.9 mb, ~20.8 km), the spectral density of the eastward moving component (period 10–30 days) attains its maximum over the equator, being consistent with the identification of this component as Kelvin waves observed by Wallace and Kousky (1968). On the other hand, the spectral density of the westward moving component (period 10–30 days) attains its minimum over the equator, being consistent with the identifi-

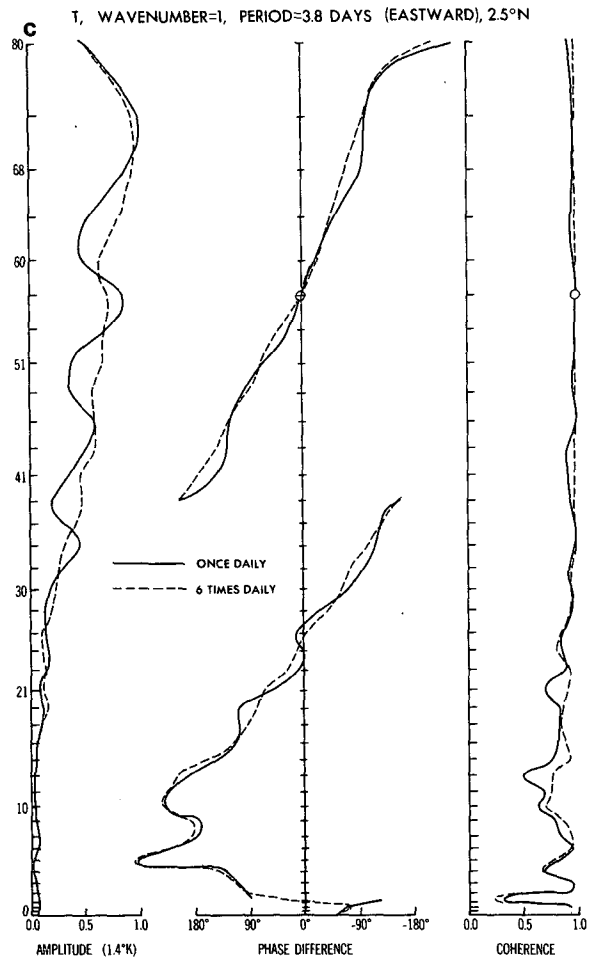

FIG. 8. (*Continued*)

cation of this component as a Rossby mode. Fig. 10b (2.1 mb, ~42.9 km) and Fig. 10c (0.3 mb, ~56.8 km) are similar to Fig. 10a except that the spectral density of the eastward moving components has peaks at shorter periods around 6 days and 3.5 days corresponding to the shorter period Kelvin waves. It should also be noted that shorter period components are associated with broader meridional widths as in Salby *et al.* (1984). These extents are in agreement with observations but are somewhat small compared to theoretical expectations in the absence of a basic flow (see Salby *et al.*, 1984, Table 1).

The latitudinal structure of the three types of Kelvin waves is illustrated in Fig. 11. Figure 11a shows the latitudinal distributions (at 47.9 mb, ~20.8 km) of the space–time amplitude, phase difference and coherence of the zonal and meridional components for wavenumber 1 and an eastward moving period of 15 days. The zonal component has a much larger amplitude than the meridional component and attains its maximum at the equator, in agreement with the observed (Wallace and Kousky, 1968) and theoretical (Matsuno, 1966) Kelvin wave. The zonal component is associated with little phase variation between 12.5°S and 12.5°N and does not change its sign (symmetric) across the equator. The coherence with respect to the equator is close to 1.0 between these latitudes (12.5°S–12.5°N).

Figure 11b is the same as Fig. 11a except for an eastward moving period of 5 days and at the level 2.1 mb (~42.9 km). The latitudinal structure looks similar to that of Fig. 11a although the amplitude of the zonal component has a weak but local minimum at the equator probably due to aliasing errors. Fig. 11c is the same as Fig. 11a except for an eastward moving period of 3.75 days and at the level 0.3 mb (~56.8 km). The latitudinal structure is more similar to Fig. 11b than Fig. 11a. These figures again show that the meridional extent increases with the frequency.

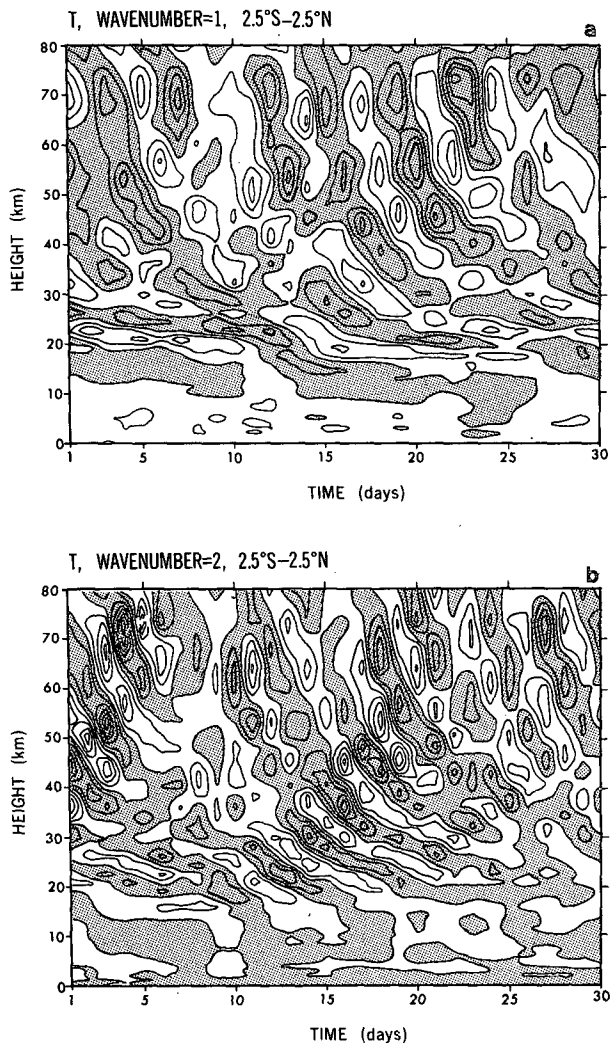

FIG. 9. Time–height distribution of the wavenumber (a) 1 and (b) 2 components of temperature at 0° longitude averaged over 2.5°S–2.5°N. Contour intervals 1 K. Shading indicates positive values.

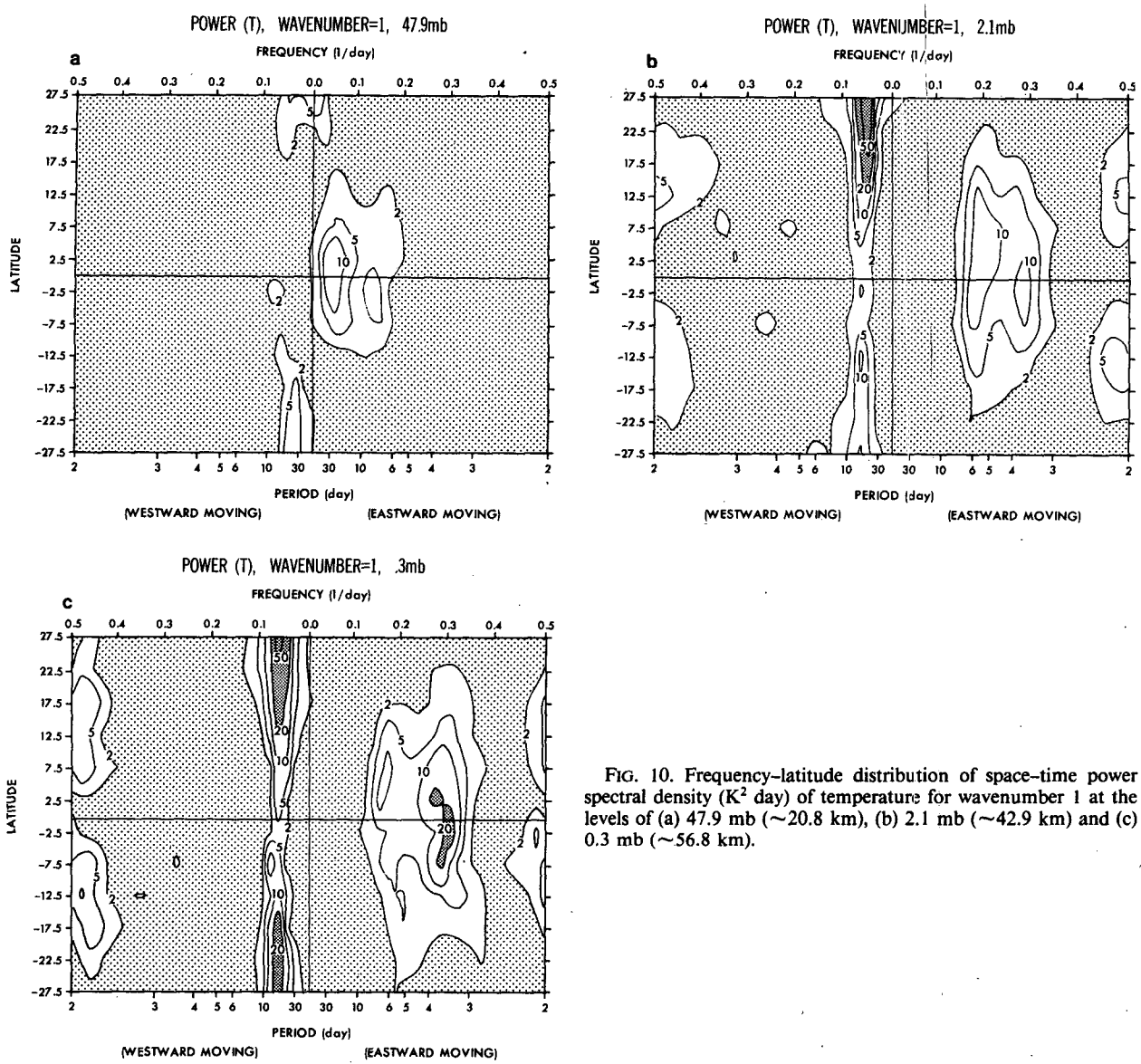

FIG. 10. Frequency–latitude distribution of space–time power spectral density (K^2 day) of temperature for wavenumber 1 at the levels of (a) 47.9 mb (~20.8 km), (b) 2.1 mb (~42.9 km) and (c) 0.3 mb (~56.8 km).

3. Analysis of six-times-daily data

The spectral analysis of once-daily data is restricted to periods longer than two days. It is also of interest to examine high-frequency waves with periods shorter than two days by the use of the six-times-daily data. For convenience, the space–time spectra are estimated by the lag correlation method using a maximum lag of 7.5 days, a rather broad frequency-width of 1/15 days and the Nyquist period of 0.33 days.

Figure 12 shows the wavenumber-frequency spectral distribution (wavenumber ≤ 30, period ≥ 0.33 days) of the traveling and standing parts of the space–time power spectra of temperature (0.03 mb, ~73.4 km) which are averaged over 7.5°S–7.5°N. The traveling and standing parts (Hayashi, 1977b) are defined in the Appendix. The "traveling waves" are defined as consisting of eastward and westward moving components which are incoherent with each other, while the "standing waves" are defined as consisting of coherent eastward and westward moving components of equal amplitudes and are associated with nodes and antinodes. The traveling and standing waves are assumed to be of different origin and are incoherent.

The eastward moving components of the traveling part (Fig. 12a) are associated with a spectral peak at wavenumber 2 and a period of three days (see Fig. 2b) corresponding to the observed mesospheric Kelvin waves (Fig. 3) found by Salby *et al.* (1984). The power spectrum also spreads from this peak toward higher wavenumber-frequency regions. This spread may be due to Kelvin waves with constant frequency-wave-

number ratio whose dispersion line is indicated in Fig. 12a. The westward moving components of the traveling part are associated with periods ~ 0.7–2 days and spread over a wide range of wavenumbers. These components may be due to westward moving gravity waves. It should be remarked that this model has no externally forced diurnal oscillations. The narrow range of the wave frequency suggests that the meridional and/or vertical wavenumbers vary with zonal wavenumbers due to the dispersion relation for Kelvin and gravity waves.

The standing part (Fig. 12b) is of smaller magnitude than the traveling part of low wavenumbers. This magnitude might even be reduced with an increasing number of time data since a short time-record tends to overestimate coherence.

Figure 13 shows the wavenumber-frequency spectral distribution (wavenumber < 30, period > 0.33 days) of the vertical flux of zonal momentum ($-\overline{u'\omega'}$) at 2.5°N and the 70.6 km level. The positive momentum flux associated with eastward moving periods is counterbalanced by the negative flux associated with westward moving periods except for those periods longer than two days. The fact that the high-frequency eastward and westward moving waves are associated with positive and negative momentum flux suggests that these equatorial waves are gravity wave modes such as studied theoretically by Lindzen and Matsuno (1968).

It is of interest to compare the vertical momentum transport by Kelvin and gravity waves. Table 1 shows the height distribution at 2.5°N of the vertical eddy momentum flux $-u'\omega'$, consisting of all the resolvable wavenumbers (1–30). The total flux consists of stationary (30-day mean) and transient (deviation from the 30-day mean) disturbances. The transient disturbances are further split into eastward and westward moving components with periods longer and shorter than two days. According to this table, the vertical eddy momentum flux above 18.3 km is primarily due to transient disturbances, while the flux due to stationary disturbances dominates below this level. The stationary disturbances are probably removed by easterlies (see Fig. 1) around the 20 km level. The eastward moving (period > 2 days) waves transport eastward momentum upward ($-\overline{u'\omega'} > 0$) above the 9.4 km standard height level, being consistent with their identification as Kelvin waves. Above 18.3 km these waves dominate over the westward moving (period > 2 days) components which transport westward momentum upward ($-\overline{u'\omega'} < 0$) between the 6.8 km and 52.5 km levels. On the other hand, the eastward (westward) moving components with periods shorter than two days transport eastward (westward) momentum upward above 12.2 km, being consistent with their identification as gravity waves. These momentum transports almost cancel each other but result in a net westward momentum flux above the 29.0 km level. The reversal of the sign of the vertical momentum flux suggests that the energy source of the transient disturbances is in the upper troposphere.

Table 2 shows the height distribution (2.5°N) of $-\partial\overline{u'\omega'}/\partial p$. According to this table, stationary waves are primarily responsible for the momentum flux divergence between the 12.9 and 16.0 km levels, while eastward moving Kelvin waves with period > 2 days are primarily responsible for the eastward force (momentum flux convergence) above the 16.0 km level. The westward and eastward moving waves with periods shorter than two days, which are primarily due to gravity waves, produce westward and eastward forces, respectively, above 16.0 km. Although these westward and eastward forces almost cancel each other, their net westward force is comparable to that of the Kelvin waves with periods > 2 days as illustrated by Fig. 14. In particular, the westward force due to the short period waves dominates over the Kelvin wave eastward force above 68.3 km, resulting in a net westward force of the zonal flow. It is of interest to note that this westward force is consistent with the westward force due to gravity waves above the level of westerlies as suggested theoretically by Lindzen (1981) and Matsuno (1982) and observationally by Vincent and Reid (1983), although gravity waves with horizontal scale shorter than ~1000 km are not resolved by the present model.

It should be remarked that the "effective vertical momentum flux convergence" is a more appropriate measure of zonal force than the vertical momentum flux convergence as suggested by Lindzen (1970) for equatorial waves. This effective flux is the vertical component of Eliassen–Palm flux as generalized by Andrews and McIntyre (1976). For Kelvin and gravity waves these vertical momentum fluxes are approximately equal as demonstrated in Andrews *et al.* (1983), since $\bar{f}\overline{v'T'}$ is negligible near the equator where both the Coriolis parameter f and the sensible heat flux $\overline{v'T'}$ are small. For Rossby waves, however, the vertical momentum flux convergence does not represent the primary component of the Eliassen–Palm flux convergence. Andrews and McIntyre (1976) suggested that stationary Rossby waves might account for the easterly acceleration to the tropical lower stratosphere, while Lindzen and Tsay (1975) had earlier attributed it to gravity waves with periods 4–6 days and a vertical wavelength which is too short (<2 km) to be observationally detectable. It is, however, beyond the scope of the present paper to compare the relative roles of the stationary and gravity waves found in the present model.

4. Conclusions and remarks

On the basis of a space–time spectral analysis of a 40-level, 5° latitude mesh GFDL general circulation model with annual mean conditions, the following results have been obtained:

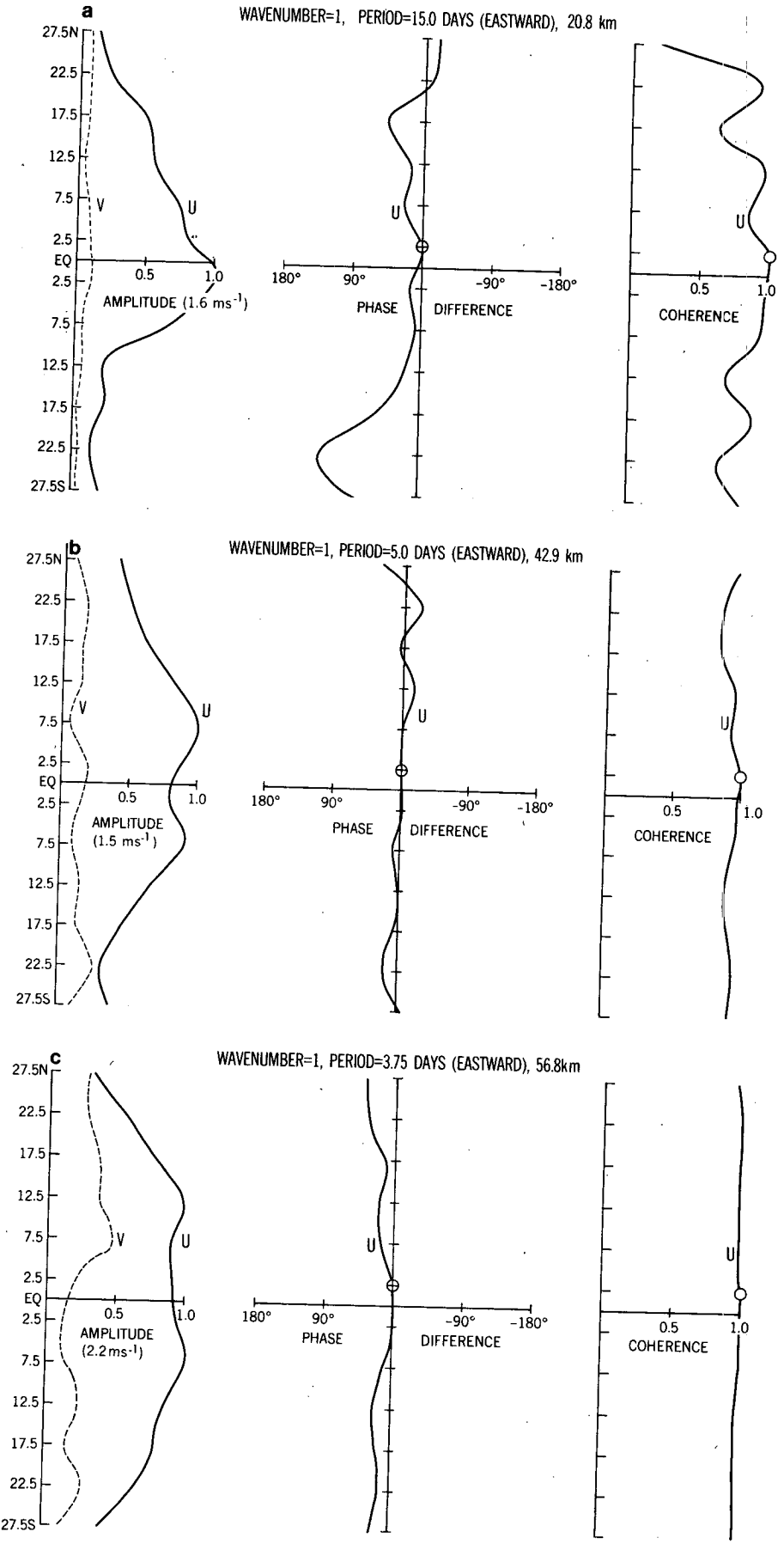
a
WAVENUMBER=1, PERIOD=15.0 DAYS (EASTWARD), 20.8 km
27.5N
22.5
17.5
12.5
7.5
2.5
EQ
2.5
7.5
12.5
17.5
22.5
27.5S
V
U
0.5
1.0
AMPLITUDE (1.6 ms-1)
U
180°
90°
-90°
-180°
PHASE
DIFFERENCE
U
0.5
1.0
COHERENCE
b
WAVENUMBER=1, PERIOD=5.0 DAYS (EASTWARD), 42.9 km
27.5N
22.5
17.5
12.5
7.5
2.5
EQ
2.5
7.5
12.5
17.5
22.5
27.5S
V
U
0.5
1.0
AMPLITUDE
(1.5 ms-1)
U
180°
90°
-90°
-180°
PHASE
DIFFERENCE
U
0.5
1.0
COHERENCE
c
WAVENUMBER=1, PERIOD=3.75 DAYS (EASTWARD), 56.8km
27.5N
22.5
17.5
12.5
7.5
2.5
EQ
2.5
7.5
12.5
17.5
22.5
27.5S
V
U
0.5
1.0
AMPLITUDE
(2.2ms-1)
U
180°
90°
-90°
-180°
PHASE
DIFFERENCE
U
0.5
1.0
COHERENCE

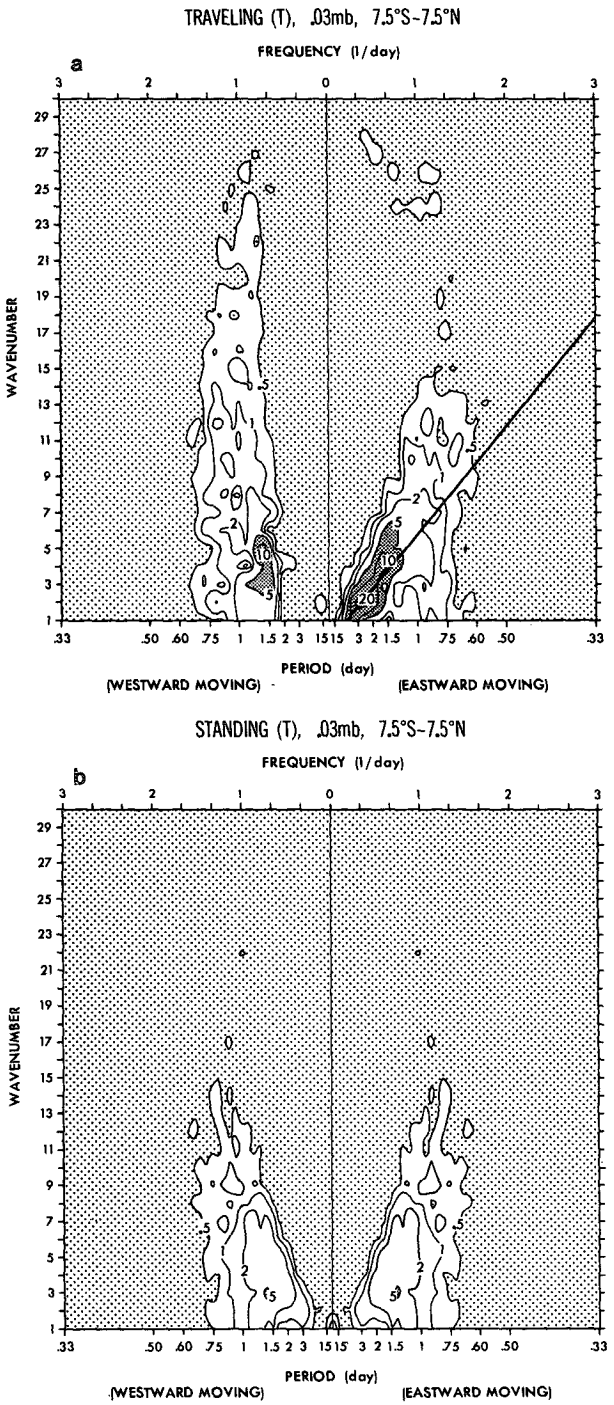

FIG. 12. Wavenumber–frequency spectral distribution (wavenumber ≤ 30, period ≥ 0.33 days) of the (a) traveling and (b) standing parts of the space-time power spectral density (K^2 day) of temperature (0.03 mb, ~73.4 km) which are averaged over 7.5°S–7.5°N. The slanted line in (a) indicates one of the dispersion lines of Kelvin waves with the same vertical wavenumber.

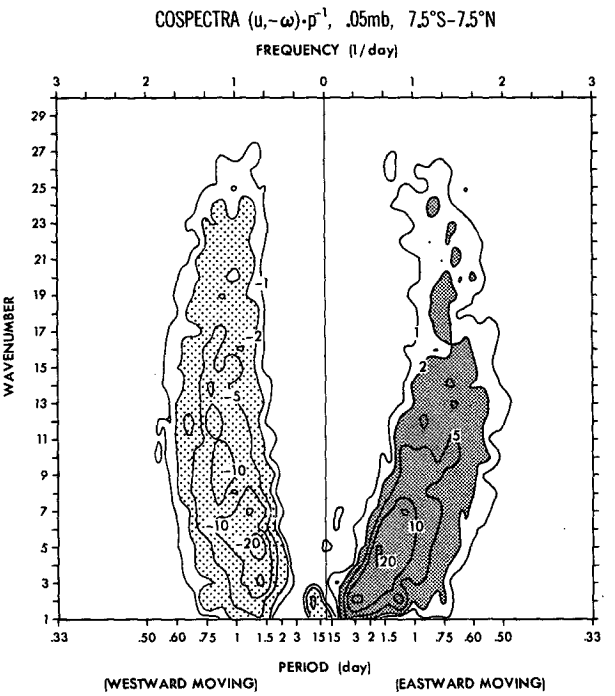

FIG. 13. Wavenumber–frequency spectral distribution (wavenumber ≤ 30, period ≥ 0.33 days) of the cospectral density (10^{-6} m s^{-2} day) of the vertical flux of zonal momentum ($-\overline{u'\omega'}p^{-1}$) at 0.05 mb ($\approx$70.6 km) averaged over 7.5°S–7.5°N.

1) The stratospheric and mesospheric Kelvin waves are associated with wavenumbers 1–2, an eastward phase velocity, an eastward tilt with height and an extremely small meridional velocity. These waves propagate vertically as a wave group.

2) The lower stratospheric Kelvin wave is associated with periods of 10–30 days (15–46 m s^{-1}) for wavenumber 1 and a vertical wavelength of ~10 km, in agreement with observations by Wallace and Kousky (1968).

3) The upper stratospheric Kelvin wave is associated with periods of 5–7 days (66–92 m s^{-1}) for wavenumber 1 and a vertical wavelength of ~20 km, in agreement with observations by Hirota (1980) and Salby *et al.* (1984).

4) The mesospheric Kelvin wave is associated with a 3–4 day period (115–154 m s^{-1}) for wavenumber 1 and a vertical wavelength of ~40 km, in agreement with that observed by Salby *et al.* (1984).

5) All these Kelvin waves are associated with an upward flux of energy and momentum and contribute to the maintenance of the eastward flow, being consistent with Eliassen–Palm diagnostics of the present model by Andrews *et al.* (1983). Their vertical mo-

FIG. 11. Latitudinal distributions of space–time amplitude, phase difference and coherence of the zonal (solid) and meridional (dashed) components (wavenumber 1). The units of amplitude over frequency width 30^{-1} day^{-1} are parenthesized. The reference latitude (2.5°N) is indicated by circles. Eastward moving period of 15 days at (a) 47.9 mb (~20.8 km), 5 days at (b) 2.1 mb (~42.9 km) and 3.75 days at (c) 0.3 mb (~56.8 km).

TABLE 1. Height distribution (2.5°N) of the vertical eddy momentum flux $-\overline{u'\omega'}$ (wavenumbers 1–30) in units of 10^{-5} m s^{-1} mb s^{-1}. The total flux consists of stationary (30-day mean) and transient (deviation from the 30-day mean) disturbances. The transient flux consists of eastward and westward moving components with periods longer and shorter than two days.

Level (km) (standard height)	Total	Stationary 30-day mean	Transient (>2 days)		Transient (<2 days)	
			Westward	Eastward	Westward	Eastward
76.1	−0.03	0.00	0.00	0.03	−0.24	0.18
66.0	−0.09	−0.00	0.01	0.12	−1.15	0.93
58.5	0.00	0.00	0.01	0.30	−2.00	1.69
52.5	0.13	0.02	−0.05	0.46	−2.82	2.53
46.6	0.27	0.02	−0.17	0.63	−3.66	3.44
41.7	−0.58	0.01	−0.54	0.89	−4.94	4.00
37.1	−1.78	0.03	−1.12	1.15	−6.76	4.93
32.9	−2.02	0.06	−1.52	1.77	−8.51	6.18
29.0	−0.53	0.18	−2.13	3.09	−10.01	8.44
25.2	4.03	0.06	−2.75	5.88	−11.59	12.44
21.7	10.20	−0.06	−3.33	8.35	−12.97	18.09
18.3	10.10	−0.53	−6.67	11.12	−18.00	24.16
15.2	−14.84	−29.72	−28.94	34.98	−34.54	43.39
12.2	−180.51	−122.68	−84.07	32.46	−28.44	22.29
9.4	−250.62	−175.33	−66.87	0.40	7.26	−15.28
6.8	−177.75	−77.59	−14.74	−95.31	45.43	−35.53
4.5	−67.26	8.47	59.77	−143.40	48.13	−40.23
2.5	32.53	89.26	68.68	−123.97	23.54	−24.98
1.0	6.65	35.21	33.55	−61.10	9.29	−10.31
0.2	0.78	1.29	1.60	−2.16	4.7	−0.41

mentum flux decays with height in such a way that $\overline{u'\omega'}$ divided by pressure is more or less constant in the mesosphere.

6) In addition, gravity waves with zonal wavenumbers 1–30 and periods of 0.7–2 days have been found in the equatorial stratosphere and mesosphere. Their eastward and westward moving components transport eastward and westward momentum upward and contribute to the momentum balance as much as or even more than Kelvin waves with periods longer than two days.

7) A westward moving planetary wave with wavenumber 1 and periods of 15–30 days is also detectable at all the levels and is identifiable with the 16-day external Rossby wave observed by Madden (1978).

The present model has no seasonal cycles and fails to simulate semiannual or quasi-biennial oscillations.

TABLE 2. As in Table 1 except for the convergence of vertical eddy momentum flux $-\partial\overline{u'\omega'}/\partial p$ (wavenumbers 1–30) in units of 10^{-7} m s^{-2}.

Level (km) (standard height)	Total	Stationary 30-day mean	Transient (>2 days)		Transient (<2 days)	
			Westward	Eastward	Westward	Eastward
79.9	−131	4	16	150	−1244	943
68.3	−33	−2	30	92	−907	753
60.3	94	4	−9	110	−361	350
53.7	19	6	−9	29	−208	201
48.0	15	1	−13	25	−126	127
42.9	−84	0	−36	19	−109	41
38.2	−53	0	−31	15	−82	43
34.0	1	1	−6	20	−46	31
29.9	25	2	−13	25	−24	34
26.2	58	−1	−4	32	−13	43
22.6	22	−0	−1	8	−7	22
19.2	7	−3	−16	20	−23	29
16.0	−59	−75	−48	65	−36	36
12.9	−266	−130	−76	−36	21	−46
10.1	−23	−32	36	−29	35	−33
7.4	61	98	27	−80	23	−8
5.0	64	41	53	−26	−4	−0
3.0	46	34	−10	24	−15	11
1.4	−21	−53	−38	69	−10	10
0.3	−6	−18	−20	31	−6	7

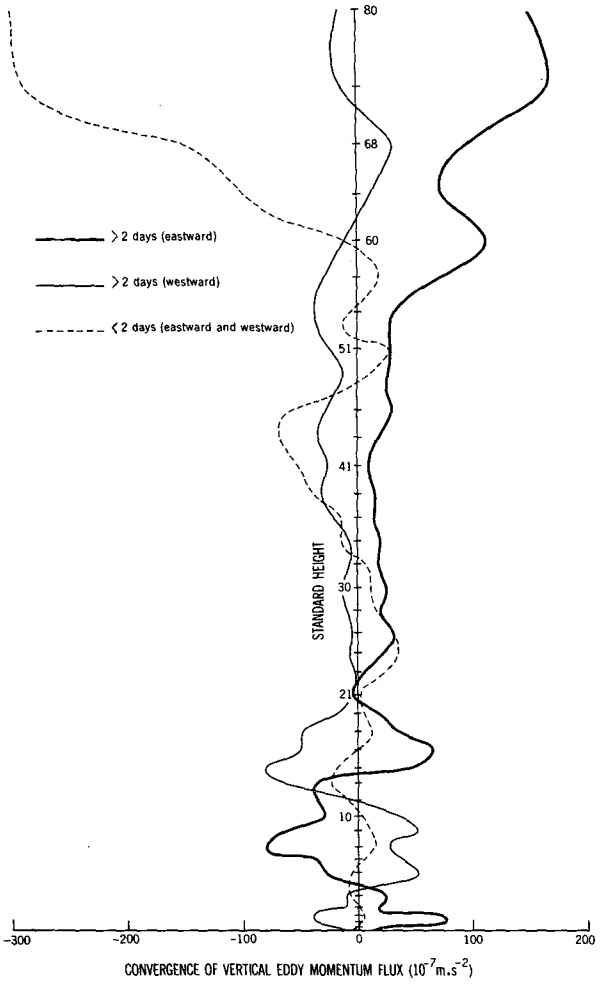

FIG. 14. Vertical distribution of the convergence (10^{-7} m s^{-2}) of the vertical flux of momentum due to transient eddies (wavenumbers 1–30) at 2.5°N. The thick (thin) solid line indicates eastward (westward) moving components with periods longer than two days, while the dashed line indicates eastward plus westward moving components with periods shorter than two days.

It is important to make a more detailed analysis of Kelvin and gravity waves simulated by a more realistic SKYHI experiment with semiannual oscillations. Such an experiment was recently conducted at GFDL (Mahlman and Umscheid, 1983) after this study was completed. It is also of interest to analyze the westward moving Rossby-gravity wave with wavenumbers ~ 3–5 and periods of ~ 4–6 days which was observed (Yanai and Maruyama, 1966) in the lower stratosphere and may be responsible for the easterly phase of the quasi-biennial oscillation as suggested theoretically by Holton and Lindzen (1972). This wave was found (Hayashi, 1974) in an 11-level GFDL model and is also detectable in the present model. Also, we would like in the future to study the effects of tropospheric forcing on these waves by extending the controlled experiments of Hayashi and Golder (1978) which were based on the 13-level GFDL model.

Acknowledgments. The authors are very grateful to Drs. M. L. Salby, I. Hirota, S. Miyahara and R. A. Plumb for their valuable comments which have led to a significant improvement of the original manuscript. Thanks are extended to J. Kennedy, P. Tunison and J. Connor for technical assistance.

APPENDIX

Standing and Traveling Waves

This appendix summarizes the method (Hayashi, 1977b) of partitioning space–time power spectra into standing and traveling wave parts which are used in the present paper.

Space–time power spectra can be partitioned into standing and traveling parts as

$$P_{k,\pm\omega}(W) = P_{k,\pm\omega}(W^s) + P_{k,\pm\omega}(W^t), \quad \text{(A1)}$$

where these parts are given by

$$P_{k,\pm\omega}(W^s) = P^{1/2}_{k,\omega}(W)P^{1/2}_{k,-\omega}(W)\mathrm{Coh}_\omega(W_h, W_{-k}), \quad \text{(A2)}$$

$$P_{k,\pm\omega}(W^t) = P_{k,\pm\omega}(W) - P_{k,\pm\omega}(W^s). \quad \text{(A3)}$$

Here, $\mathrm{Coh}_\omega(W_k, W_k)$ denotes the coherence between the eastward and westward moving components determined by

$$4[1 - \mathrm{Coh}_\omega{}^2(W_k, W_{-k})]P_{k,\omega}(W)P_{k,-\omega}(W) = [1 - \mathrm{Coh}_\omega{}^2(C_k, S_k)]P_\omega(C_k)P_\omega(S_k), \quad \text{(A4)}$$

where $\mathrm{Coh}_\omega(C_k, S_k)$ is the coherence between the zonal cosine and sine coefficients C_k and S_k.

In practice, (A.2) can be computed by the use of (A.4) as

$$2P_{k,\pm\omega}(W^s) = \{\tfrac{1}{4}[P_\omega(C_k) - P_\omega(S_k)]^2 + K^2_\omega(C_k, S_k)\}^{1/2}. \quad \text{(A5)}$$

When the maximum entropy method is used (see Hayashi, 1982), the power spectra and coherence should be computed through time MEM cross spectra as

$$4P_{k,\pm\omega}(W) = P_{\pm\omega}(F_k), \quad \text{(A6)}$$

$$\mathrm{Coh}_\omega(W_k, W_{-k}) = \mathrm{Coh}_\omega(F_k, F^*_k), \quad \text{(A7)}$$

with

$$F_k \equiv C_k - iS_k, \quad \text{(A8)}$$

where C_k and S_k are the zonal cosine and sine coefficients and the asterisk denotes the complex conjugate.

REFERENCES

Andrews, D. G., and M. E. McIntyre, 1976: Planetary waves in horizontal and vertical shear: The generalized Eliassen–Palm relation and the mean zonal acceleration. *J. Atmos. Sci.*, **33**, 2031–2048.

——, J. D. Mahlman and R. W. Sinclair, 1983: Eliassen–Palm diagnostics of wave–mean flow interaction in the GFDL "SKYHI" general circulation model. *J. Atmos. Sci.*, **40**, 2768–2784.

Dunkerton, T. J., 1979: On the role of the Kelvin wave in westerly phase of the semiannual zonal wind oscillation. *J. Atmos. Sci.*, **36**, 32–41.

——, 1982: Theory of mesopause semiannual oscillation. *J. Atmos. Sci.*, **39**, 2681–2690.

Fels, S. B., J. D. Mahlman, M. D. Schwarzkopf and R. W. Sinclair, 1980: Stratospheric sensitivity to perturbations in ozone and carbon dioxide: Radiation and dynamical response. *J. Atmos. Sci.*, **37**, 2265–2297.

Hamilton, K., 1982: Rocketsonde observations of the mesospheric semiannual oscillation of Kwajalein. *Atmos.-Ocean*, **20**, 281–286.

Hayashi, Y., 1974: Spectral analysis of tropical disturbances appearing in a GFDL general circulation model. *J. Atmos. Sci.*, **31**, 180–218.

——, 1977b: On the coherence between progressive and retrogressive waves and a partition of space–time power spectra into standing and traveling parts. *J. Appl. Meteor.*, **16**, 368–373.

——, 1981: Space-time cross spectral analysis using the maximum entropy method. *J. Meteor. Soc. Japan*, **59**, 620–624.

——, 1982: Space–time spectral analysis and its applications to atmospheric waves. *J. Meteor. Soc. Japan*, **60**, 156–171.

——, and D. G. Golder, 1978: The generation of equatorial transient planetary waves: Control experiments with a GFDL general circulation model. *J. Atmos. Sci.*, **35**, 2068–2082.

——, and ——, 1980: The seasonal variation of tropical transient planetary waves appearing in a GFDL general circulation model. *J. Atmos. Sci.*, **37**, 705–716.

——, and ——, 1983: Transient planetary waves simulated by GFDL spectral general circulation models. Part I: Effects of mountains. *J. Atmos. Sci.*, **40**, 941–950.

Hirota, I., 1978: Equatorial waves in the upper stratosphere and mesosphere in relation to the semiannual oscillation of the zonal wind. *J. Atmos. Sci.*, **35**, 714–722.

——, 1979: Kelvin waves in the equatorial middle atmosphere observed by the Nimbus 5 SCR. *J. Atmos. Sci.*, **36**, 217–222.

——, 1980: Observational evidence of the semiannual oscillation in the tropical middle atmosphere—A review. *Pure Appl. Geophys.*, **118**, 217–238.

Holton, J. R., and R. S. Lindzen, 1968: A note on "Kelvin" waves in the atmosphere. *Mon. Wea. Rev.*, **96**, 385–386.

——, and ——, 1972: An updated theory for the quasi-biennial cycle of the tropical stratosphere. *J. Atmos. Sci.*, **29**, 1076–1080.

Kousky, V. E., and J. M. Wallace, 1971: On the interaction between Kelvin waves and the mean zonal flow. *J. Atmos. Sci.*, **28**, 162–169.

Lindzen, R. S., 1970: Vertical momentum transport by large-scale disturbances of the equatorial lower stratosphere. *J. Meteor. Soc. Japan*, **48**, 81–82.

——, 1981: Turbulence and stress due to gravity wave and tidal breakdown. *J. Geophys. Res.*, **86**, 9707–9714.

——, and J. R. Holton, 1968: A theory of the quasi-biennial oscillation. *J. Atmos. Sci.*, **25**, 1095–1107.

——, and T. Matsuno, 1968: On the nature of large-scale wave disturbances in the equatorial lower stratosphere. *J. Meteor. Soc. Japan*, **46**, 215–221.

——, and C.-Y. Tsay, 1975: Wave structure of the tropical stratosphere over the Marshall Islands area during 1 April–1 July, 1958. *J. Atmos. Sci.*, **32**, 2008–2021.

Madden, R. A., 1978: Further evidence of traveling planetary waves. *J. Atmos. Sci.*, **35**, 1605–1618.

——, 1979: Observations of large-scale traveling Rossby waves, *Rev. Geophys. Space Phys.*, **17**, 1935–1949.

——, and K. Labitzke, 1981: A free Rossby wave in the troposphere and stratosphere during January 1979. *J. Geophys. Res.*, **86**, 1247–1254.

Mahlman, J. D., and R. W. Sinclair, 1980: Recent results from the GFDL troposphere–stratosphere-mesosphere general circulation model. *Collection of Extended Abstracts Presented at ICMUA Sessions and IUGG Symposium 18*, XVII IUGG General Assembly, December 1979, Canberra, 11–18. [Available from S. Ruttenberg, Secretary General, IAMAP, NCAR, P.O. Box 3000, Boulder, CO.]

——, and L. J. Umscheid, 1983: Dynamics of the middle atmosphere: Successes and problems of the GFDL "SKYHI" general circulation model. *Dynamics of the Middle Atmosphere, Advances in Earth and Planetary Sciences*, J. R. Holton and T. Matsuno, Eds., Terra Scientific Publishing, 501–525.

Manabe, S., D. C. Hahn and J. L. Holloway, Jr., 1974: The seasonal variation of the tropical circulation as simulated by a global model of the atmosphere. *J. Atmos. Sci.*, **31**, 43–83.

Matsuno, T., 1966: Quasi-geostrophic motions in the equatorial area. *J. Meteor. Soc. Japan*, **44**, 25–43.

——, 1982: A quasi-one-dimensional model of the middle atmosphere circulation interacting with internal gravity waves. *J. Meteor. Soc. Japan*, **60**, 215–226.

McIntyre, M. E., and T. N. Palmer, 1983: Breaking planetary waves in the stratosphere. *Nature*, **305**, No. 13, 593–600.

Salby, M. L., 1981: Rossby normal modes in nonuniform background configurations. Part I: Simple fields; Part II: Equinox and solstice conditions. *J. Atmos. Sci.*, **38**, 1803–1826, 1827–1840.

——, 1982: Sampling theory for asynoptic satellite observations Part I: Space-time spectra, resolution and aliasing. *J. Atmos. Sci.*, **39**, 2577–2600.

——, D. L. Hartmann, P. L. Bailey and J. C. Gille, 1984: Evidence for equatorial Kelvin modes in Nimbus-7 LIMS. *J. Atmos. Sci.*, **41**, 220–235.

Vincent, R. A., and I. M. Reid, 1983: HF Doppler measurements of mesospheric gravity wave momentum fluxes. *J. Atmos. Sci.*, **40**, 1321–1333.

Wallace, J. M., 1973: General circulation of the tropical lower stratosphere. *Rev. Geophys. Space Phys.*, **11**, 191–222.

——, and V. E. Kousky, 1968: Observational evidence of Kelvin waves in the tropical stratosphere. *J. Atmos. Sci.*, **25**, 280–292.

Yanai, M., 1975: Tropical meteorology. *Rev. Geophys. Space Phys.*, **13**, 685–710, 800–808.

——, and T. Maruyama, 1966: Stratospheric wave disturbances propagating over the equatorial Pacific. *J. Meteor. Soc., Japan*, **44**, 291–294.